

Collectivity at $N = 40$ in neutron-rich ^{64}Cr

A. Gade,^{1,2} R. V. F. Janssens,³ T. Baugher,^{1,2} D. Bazin,¹ B. A. Brown,^{1,2} M. P. Carpenter,³ C. J. Chiara,^{3,4} A. N. Deacon,⁵ S. J. Freeman,⁵ G. F. Grinyer,¹ C. R. Hoffman,³ B. P. Kay,³ F. G. Kondev,⁶ T. Lauritsen,³ S. McDaniel,^{1,2} K. Meierbachtol,^{1,7} A. Ratkiewicz,^{1,2} S. R. Stroberg,^{1,2} K. A. Walsh,^{1,2} D. Weisshaar,¹ R. Winkler,¹ and S. Zhu³

¹National Superconducting Cyclotron Laboratory, Michigan State University, East Lansing, Michigan 48824, USA

²Department of Physics and Astronomy, Michigan State University, East Lansing, Michigan 48824, USA

³Physics Division, Argonne National Laboratory, Argonne, Illinois 60439, USA

⁴Department of Chemistry and Biochemistry, University of Maryland, College Park, Maryland 20742, USA

⁵School of Physics and Astronomy, Schuster Laboratory, University of Manchester, Manchester M13 9PL, United Kingdom

⁶Nuclear Engineering Division, Argonne National Laboratory, Argonne, Illinois 60439, USA

⁷Department of Chemistry, Michigan State University, East Lansing, Michigan 48824, USA

(Received 19 March 2010; published 28 May 2010)

⁹Be-induced inelastic scattering of $^{62,64,66}\text{Fe}$ and $^{60,62,64}\text{Cr}$ was performed at intermediate beam energies. Excited states in ^{64}Cr were measured for the first time. Energies and population patterns of excited states in these neutron-rich Fe and Cr nuclei are compared and interpreted in the framework of large-scale shell-model calculations in different model spaces. Evidence for increased collectivity and for distinct structural changes between the neighboring Fe and Cr isotopic chains near $N = 40$ is presented.

DOI: [10.1103/PhysRevC.81.051304](https://doi.org/10.1103/PhysRevC.81.051304)

PACS number(s): 21.10.Re, 23.20.Lv, 25.60.-t, 27.50.+e

The shell structure of atomic nuclei is one of the central building blocks for a comprehensive description of these strongly correlated many-body quantum systems. Shell structure is fairly well understood for stable nuclei. However, significant modifications have been encountered for short-lived, exotic species with extreme ratios of proton and neutron numbers. Much progress has been made in recent years toward understanding these changes as being driven to a large extent by spin-isospin parts of the nucleon-nucleon interaction, in particular by the monopole parts of the tensor interaction [1–3]. Experimental information at the extremes of proton-neutron asymmetry is essential to benchmark the isospin dependence of this shell evolution.

The region of neutron-rich nuclei above doubly magic ^{48}Ca has provided much insight into the nature of the forces responsible for this modified shell structure. Evidence for a new subshell gap at neutron number $N = 32$ has been found [4], while neutron-rich Cr and Fe nuclei around $N = 40$ exhibit collective behavior. The description of nuclei with $N = 40$ challenges theory as they are the subject of particularly rapid structural evolution. Driven by the deformation-driving neutron $g_{9/2}$ intruder orbital, they exhibit a remarkable variation in collectivity as a function of proton number: $N = Z = 40$ ^{80}Zr is strongly deformed [5] while $Z = 28$ ^{68}Ni has a high-lying 2_1^+ state and a reduced quadrupole collectivity [6]. With just two protons less than ^{68}Ni , ^{66}Fe was the most neutron-rich $N = 40$ nucleus with measured spectroscopic information prior to the present work. Its low-lying first excited 2^+ state indicates yet another sudden change in nuclear structure with increased collectivity [7]. In its vicinity, indications for collective behavior have come from 2_1^+ energies in the Fe isotopic chain out to $^{68}\text{Fe}_{42}$ and in the Cr isotopes out to $^{62}\text{Cr}_{38}$ [7–10]. For $^{60,62}\text{Cr}$ direct evidence is also provided by the measurement of the quadrupole deformation lengths in inelastic proton scattering [11].

For the $N = 40$ isotones, the most extreme proton-neutron asymmetry reachable today occurs in ^{64}Cr , a nucleus where the onset of collectivity has been conjectured to be most pronounced and the 2_1^+ energy calculated to be the lowest in the region [8,12]. In this rapid communication, we report on the first measurement of the 2_1^+ and 4_1^+ states in this key nucleus and the resulting first experimental signatures of collectivity from $^9\text{Be}(^{64}\text{Cr}, ^{64}\text{Cr} + \gamma)X$ inelastic scattering. We also present marked structural differences between the ^{64}Cr and ^{66}Fe isotones. This confirms the occurrence of a significant change in nuclear structure between ^{66}Fe and ^{64}Cr as suggested recently from the small cross section for the two-proton knockout reaction, $^9\text{Be}(^{66}\text{Fe}, ^{64}\text{Cr})X$ [10].

The measurement was performed at the National Superconducting Cyclotron Laboratory (NSCL) using $^{60,62,64}\text{Cr}$ and $^{62,64,66}\text{Fe}$ secondary beams produced by fragmentation of a 130 MeV/u ^{76}Ge primary beam. Six different settings of the A1900 fragment separator [13] were used to deliver these secondary beams onto a 370 mg/cm² thick ^9Be foil located at the target position of the large-acceptance S800 spectrograph [14]. The A1900 separator was operated at a 3% total momentum acceptance, except for the ^{62}Fe and ^{62}Cr settings, where smaller momentum widths were transmitted. Specifically, for ^{64}Cr , a 399 mg/cm² ^9Be production target was used with a 150 mg/cm² Al wedge located at the midpoint of the separator to purify the secondary beam. The respective midtarget energies in the ^9Be reaction target were 73.0, 67.5, and 82.6 MeV/u for $^{62,64,66}\text{Fe}$ and 80.6, 74.6, and 87.0 MeV/u for $^{60,62,64}\text{Cr}$, respectively. Particle identification was achieved event-by-event with the S800 focal-plane detection system [14]. The energy loss measured by the S800 ionization chamber and the time-of-flight information between plastic scintillators—corrected for the angle and momentum of each ion—were used to identify unambiguously the reaction residues emerging from the target. The particle-identification

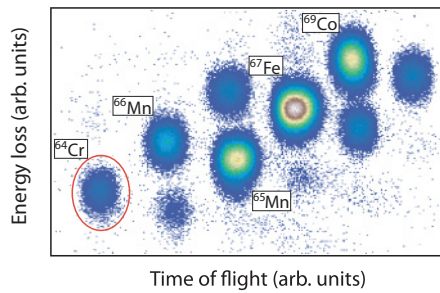


FIG. 1. (Color online) Particle-identification spectrum for the cocktail beam optimized for ^{64}Cr . The energy loss measured in the S800 ionization chamber is plotted versus the ion's time of flight. ^{64}Cr and the four most intense constituents of the beam are labeled.

spectrum for ^{64}Cr is provided in Fig. 1. The beam-on-target time amounted to about 110 h.

The target was surrounded by the high-resolution γ -ray detection system SeGA, an array of 32-fold segmented HPGe detectors [15]. The segmentation enabled event-by-event Doppler reconstruction of the γ rays emitted in flight by the reaction residues. The emission angle for the Doppler reconstruction was determined from the location of the segment with the largest energy deposition. Fifteen detectors were arranged in two rings at central angles of 90° (eight detectors) and 37° (seven detectors) with respect to the beam axis. The photopeak efficiency of the array was determined with standard sources and corrected for the Lorentz boost for γ -ray emission from nuclei moving at about 35% of the speed of light.

Figures 2 and 3 show event-by-event Doppler reconstructed γ -ray spectra detected in coincidence with scattered projec-

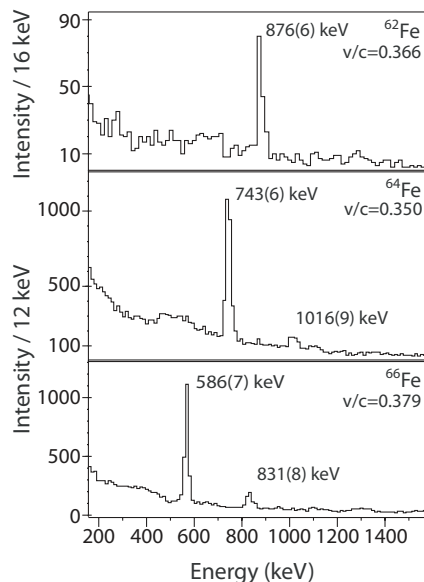


FIG. 2. Event-by-event Doppler-reconstructed γ -ray spectra detected in coincidence with scattered $^{62,64,66}\text{Fe}$ projectiles. The dominant peak in each spectrum corresponds to the decay of the first 2^+ level to the ground state. The $4_1^+ \rightarrow 2_1^+$ transition is clearly visible in ^{64}Fe and ^{66}Fe . In ^{62}Fe there is an excess of counts at the known $4_1^+ \rightarrow 2_1^+$ transition energy but a peak structure is not clearly identifiable.

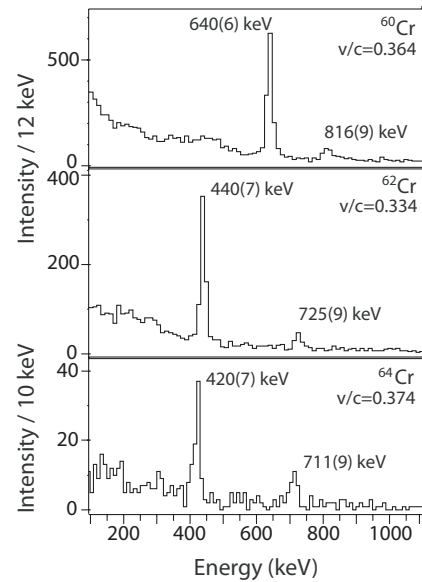


FIG. 3. Event-by-event Doppler-reconstructed γ -ray spectra detected in coincidence with scattered $^{60,62,64}\text{Cr}$ projectiles. The dominant peak in each spectrum corresponds to the decay of the first 2^+ level to the ground state; the known $4_1^+ \rightarrow 2_1^+$ transition is clearly visible in ^{60}Cr and ^{62}Cr . The γ -ray transitions at 420(7) keV and 711(9) keV observed in ^{64}Cr are new and assigned to the $2_1^+ \rightarrow 0_1^+$ and $4_1^+ \rightarrow 2_1^+$ decays, respectively.

tiles. For $^{62,64,66}\text{Fe}$ and $^{60,62}\text{Cr}$, the 2_1^+ and 4_1^+ levels are known [7–10] and these states are populated in the ^9Be -induced inelastic scattering with a distinct population pattern. In coincidence with ^{64}Cr , two γ -ray transitions were detected with energies $E_\gamma = 420(7)$ keV and $711(9)$ keV. This establishes the energy of the 2_1^+ and 4_1^+ states as $E(2_1^+) = 420(7)$ keV and $E(4_1^+) = 1131(11)$ keV, based on the consistent population patterns observed for all reactions used here. This constitutes the first observation of excited states in this neutron-rich $N = 40$ nucleus.

Figure 4 compares the experimental 2_1^+ energies and the $R_{4/2} = E(4_1^+)/E(2_1^+)$ ratios to results from the projected shell model (PSM) [16,17] and the spherical shell model calculations with the fp and the fp_g model spaces. The fp shell-model calculations were performed with the code NUSHELL and used the GXPF1A effective interaction that is successful in accounting for the emergence of the $N = 32$ subshell gap [18]. The results from the fp_g shell model are taken from Ref. [19] for the Cr isotopes and from Ref. [16] for Fe. For Cr, the large-scale spherical shell model calculations use the pairing plus multipole forces with the monopole interaction included [19–21]. The fp_g model space in this approach comprises the $0f_{7/2}$, $1p_{3/2}$, $0f_{5/2}$, and $1p_{1/2}$ active proton orbitals and the $0f_{7/2}$, $1p_{3/2}$, $0f_{5/2}$, $1p_{1/2}$, and $0g_{9/2}$ neutron orbitals with eight neutrons frozen in the $f_{7/2}$ orbital [19]. For Fe, results from PSM calculations are also provided in Fig. 4. This approach uses a deformed basis deduced from the deformed Nilsson model and configuration mixing introduced on a projected, smaller basis, allowing for the incorporation of large model spaces, cross-shell excitations, and collective motion [16]. The PSM results shown in Fig. 4 include

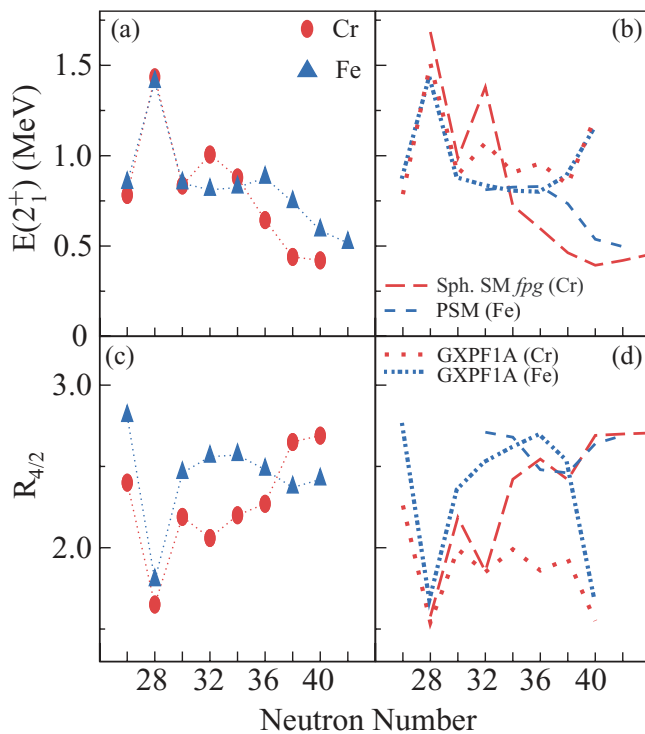


FIG. 4. (Color online) Experimental 2_1^+ excitation energies and $R_{4/2}$ ratios for the even-even Cr and Fe isotopes (left) compared to PSM and spherical shell model calculations in the fp and fp shell model spaces (see text for details).

three major harmonic oscillator shells for both neutrons and protons in Fe. The fp shell-model calculation with the GXPF1A Hamiltonian does not include the $\nu g_{9/2}$ orbital and, consequently, predicts high-lying 2_1^+ states associated with a sizable $N = 40$ subshell gap at ^{64}Cr and ^{66}Fe in this model space [Fig. 4(b)]. The inclusion of the $g_{9/2}$ orbital for Cr and the use of the PSM starting from a deformed basis for Fe reproduce the experimental observations, in particular the decreasing 2_1^+ energies at $N = 40$ in Cr and beyond 40 in the Fe isotopic chain. The fp shell-model calculation by Kaneko *et al.* [21] predicts the 2_1^+ energy in ^{64}Cr to within 30 keV. It is worth noting that the fp shell model calculation by Caurier *et al.* [12], which includes the $\nu d_{5/2}$ orbital as well, agrees with the fp shell model calculations for Cr within 100 and 150 keV at $N = 38$ and 40 and $N = 36$, respectively. It also agrees within less than 100 and 130 keV with the PSM calculations for Fe at $N = 36$ and 38 and $N = 40$, respectively.

The $R_{4/2}$ ratio of level energies provides a convenient classification of structural properties in terms of noncollective (<2.0), spherical-vibrational (~ 2.0), transitional (~ 2.5), or rigid-rotor (~ 3.33) regimes. As can be concluded from Fig. 4(c), this $R_{4/2}$ ratio increases steeply toward a transitional character between $N = 30$ and 40 in the Cr isotopic chain. In contrast, it remains constant and even decreases slightly in the corresponding Fe chain. Figure 4(d) provides the calculated $R_{4/2}$ ratios. The GXPF1A interaction reproduces the distinct dip at the $N = 32$ shell gap in Cr, but fails for higher neutron numbers because of the absence of the $g_{9/2}$ orbit in the Hamiltonian. On the other hand, the fp shell model and

PSM calculations provide an adequate description of the data: the PSM results match the $R_{4/2}$ results for Fe reasonably well, while the spherical fp shell model predicts the correct value for ^{64}Cr , but deviates by 0.4–0.5 for the lighter Cr nuclei. This difference in performance of the two models can likely be attributed to the omission of the $\nu d_{5/2}$ orbit in the fp model space and its implicit inclusion in the PSM approach. It was indeed shown by Caurier *et al.* [12] and Sorlin *et al.* [8] that the $d_{5/2}$ orbit may play an important role in the description of quadrupole collectivity in this region.

The reaction chosen, ^9Be -induced inelastic scattering of fast, exotic projectiles, offers advantages as well as disadvantages compared to the more traditional approach of intermediate-energy Coulomb excitation. In the latter, projectiles are excited in the electromagnetic field of a high- Z nucleus, for example, Au, and in medium-heavy even-even nuclei typically only the first 2_1^+ state is excited in a single step [22]. The measured excitation cross section can then be translated into a $B(E2)$ transition strength that is a measure of quadrupole collectivity and can be readily compared to predictions of nuclear models [23]. However, prompt, low-energy in-beam γ -ray background, such as bremsstrahlung induced by the interaction with the high- Z target, can obscure low-energy γ -ray transitions ($E_\gamma < 600$ keV). In ^9Be -induced inelastic scattering, the strongly Z -dependent, low-energy component of the in-beam background is avoided, leading to the favorable peak-to-background conditions (Figs. 2 and 3) needed in the regime of low excitation energy and low statistics of the present measurement. Furthermore, in scattering processes from low- Z targets, the nuclear interaction dominates over the Coulomb one and allows for the excitation of states beyond the 2_1^+ level, resulting here in the identification of the 4_1^+ state in ^{64}Cr . At present, the theoretical details of the potentials and couplings in the ^9Be -induced inelastic scattering process have not yet been explored and, as a result, the measured excitation cross sections cannot be readily translated into quantities to be confronted with nuclear structure calculations.

It is nevertheless worthwhile to investigate the relative behavior of the measured excitation cross sections. Higher-lying excited states are likely also populated in the inelastic scattering process and these levels can be expected to decay predominantly toward the yrast 2_1^+ and 4_1^+ states. Hence, the cross section for observing the $2_1^+ \rightarrow 0_1^+$ γ -ray transition $\sigma^*(2_1^+)$ a quantity including both observed and unobserved feeding can be viewed as an integrated measure of the excitability of the nuclei in the scattering process. Figure 5 presents this quantity normalized to ^{62}Fe . The difference in trend for the Fe and Cr isotopic chains is rather striking: While $\sigma^*(2_1^+)$ is essentially constant for all Fe isotopes and comparable to the value for ^{60}Cr , it increases by 25% for ^{62}Cr ($N = 38$) and doubles for ^{64}Cr ($N = 40$), relative to ^{60}Cr . Although the description of the reaction mechanism is a challenge for the future, one may speculate that the change in trend indicates a corresponding change in the collective behavior of Cr nuclei toward $N = 40$. A similar evolution is then not present in the Fe chain. Similarly, a distinct change in nuclear structure between ^{66}Fe and ^{64}Cr was inferred from the small cross section for the two-proton knockout reaction,

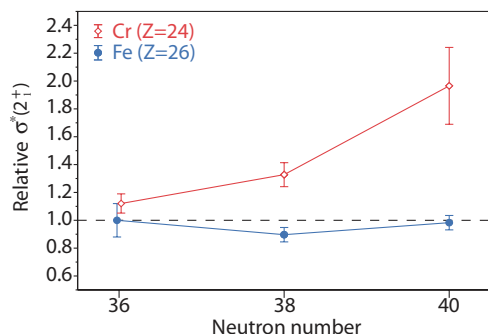


FIG. 5. (Color online) Excitation cross sections relative to ^{62}Fe for observing the $2_1^+ \rightarrow 0_1^+$ γ -ray transition, $\sigma^*(2_1^+)$, including both observed and unobserved feeding, measured for $^{60,62,64}\text{Cr}$ and $^{62,64,66}\text{Fe}$ on ^9Be .

$^9\text{Be}(^{66}\text{Fe}, ^{64}\text{Cr})X$, attributed to a lack of overlap between the ^{66}Fe ground state and the final states in the ^{64}Cr residue [10].

In summary, level energies and excitation cross sections for ^9Be -induced inelastic scattering of $^{62,64,66}\text{Fe}$ and $^{60,62,64}\text{Cr}$ were measured at intermediate beam energies. For the first time, excited states in ^{64}Cr are reported. Large-scale shell model calculations including the $\nu g_{9/2}$ intruder orbital reproduce the excitation spectra. A distinct change in the trend of the population of the 2_1^+ states in the Cr isotopic chain compared to the Fe isotones has been interpreted in terms of structural differences at $N = 40$.

We thank Dr. Kazunari Kaneko and Dr. Yang Sun for providing us with the numerical results of the Cr and Fe excitation energies from the figures in Refs. [16,19]. This work was supported by the National Science Foundation under Grants PHY-0606007 and PHY-0758099; by the US Department of Energy, Office of Nuclear Physics, under Contract No. DE-AC02-06CH11357; and by the UK Science and Technology Facilities Council (STFC).

-
- [1] T. Otsuka *et al.*, *Phys. Rev. Lett.* **87**, 082502 (2001).
 [2] T. Otsuka *et al.*, *Phys. Rev. Lett.* **95**, 232502 (2005).
 [3] T. Otsuka *et al.*, *Phys. Rev. Lett.* **104**, 012501 (2010).
 [4] J. I. Prisciandaro *et al.*, *Phys. Lett. B* **510**, 17 (2001); R. V. F. Janssens *et al.*, *ibid.* **546**, 55 (2002); D.-C. Dinca *et al.*, *Phys. Rev. C* **71**, 041302(R) (2005).
 [5] C. J. Lister *et al.*, *Phys. Rev. Lett.* **59**, 1270 (1987).
 [6] O. Sorlin *et al.*, *Phys. Rev. Lett.* **88**, 092501 (2002).
 [7] M. Hannawald *et al.*, *Phys. Rev. Lett.* **82**, 1391 (1999).
 [8] O. Sorlin *et al.*, *Eur. Phys. J. A* **16**, 55 (2003).
 [9] S. Zhu *et al.*, *Phys. Rev. C* **74**, 064315 (2006).
 [10] P. Adrich *et al.*, *Phys. Rev. C* **77**, 054306 (2008).
 [11] N. Aoi *et al.*, *Phys. Rev. Lett.* **102**, 012502 (2009).
 [12] E. Caurier *et al.*, *Eur. Phys. J. A* **15**, 145 (2002).
 [13] D. J. Morrissey *et al.*, *Nucl. Instrum. Methods Phys. Res. B* **204**, 90 (2003).
 [14] D. Bazin *et al.*, *Nucl. Instrum. Methods Phys. Res. B* **204**, 629 (2003).
 [15] W. F. Mueller *et al.*, *Nucl. Instrum. Methods Phys. Res. A* **466**, 492 (2001).
 [16] Yang Sun *et al.*, *Phys. Rev. C* **80**, 054306 (2009).
 [17] K. Hara and Y. Sun, *Int. J. Mod. Phys. E* **4**, 637 (1995).
 [18] M. Honma *et al.*, *Phys. Rev. C* **65**, 061301(R) (2002); *Eur. Phys. J. A* **25** s1, 499 (2005).
 [19] K. Kaneko, Y. Sun, M. Hasegawa, and T. Mizusaki, *Phys. Rev. C* **78**, 064312 (2008).
 [20] M. Hasegawa, K. Kaneko, and S. Tazaki, *Nucl. Phys. A* **688**, 765 (2001).
 [21] K. Kaneko, M. Hasegawa, and T. Mizusaki, *Phys. Rev. C* **66**, 051306(R) (2002).
 [22] T. Glasmacher, *Annu. Rev. Nucl. Part. Sci.* **48**, 1 (1998).
 [23] A. Gade and T. Glasmacher, *Prog. Part. Nucl. Phys.* **60**, 161 (2008).